Journal of Science Research and Reviews
PRINT ISSN: 1595-9074
E-ISSN: 1595-8329
DOI: https://doi.org/10.70882/josrar.2026.v3i6.249
Homepage: https://josrar.esrgngr.org
Original Research Article

Geostatistical Evaluation and Spatial Mapping of Structural Soil Fertility in Wukari Urban Area, Taraba State, Nigeria

Waizah Yakub[1], Adashu Tanko Gani[1], Yasin Awwal Agonu[1]

[1]Department of Soil Science and Land Resources Management, Faculty of Agriculture, Federal University Wukari, Taraba State, Nigeria
*Corresponding Author's email:

KEYWORDS
Soil Fertility,
Spatial Modelling,
Principal Component Analysis,
Macronutrients,
Kriging

ABSTRACT
Soil fertility is a fundamental determinant of agricultural productivity, environmental sustainability, and urban land-use management. In urban areas such as Wukari, Taraba State, Nigeria, soil properties may vary considerably due to differences in land use, human activities, and natural soil-forming processes. Understanding these variations is essential for effective soil management and sustainable land development. However, assessing soil fertility using individual soil properties may not adequately capture the complex interactions among soil nutrients, exchangeable bases, organic matter, and salinity indicators. This study evaluates the multivariate and spatial structure of soil fertility in the Wukari urban area, Nigeria, using an integrated geostatistical framework. Seventy soil samples were analyzed for exchangeable bases, organic matter, macronutrients, and salinity indicators. Principal component analysis revealed that the first component (31.6% of total variance) was strongly dominated by exchangeable Ca (0.903), effective cation exchange capacity (0.901), and total exchangeable bases (0.891), forming the basis of a PCA-derived Soil Fertility Index. Sensitivity testing confirmed structural dependence of the index on exchange-complex variables, with substantial instability upon removal of Ca or ECEC. Semivariogram modeling indicated moderate spatial dependence for exchange variables (nugget-to-sill ratios ≈ 76–77%) and short-range strong dependence for total nitrogen and available phosphorus. The Soil Fertility Index exhibited weak-to-moderate spatial structure (nugget/sill = 76.1%) under a Stable model with a range of 17.6 km. Global Moran's I statistics were low (≤0.05), indicating scale-dependent heterogeneity and patch-level spatial continuity rather than regional clustering. Cross-validation showed unbiased kriging predictions with mean error approaching zero and root mean square standardized values near unity. The results demonstrate that fertility gradients are exchange-capacity-driven and spatially fragmented, highlighting the importance of multivariate geostatistical integration in urban soil fertility assessment.

CITATION
Waizah, Y., Tanko, A., & Agono, Y. (2026). GEOSTATISTICAL EVALUATION AND SPATIAL MAPPING OF STRUCTURAL SOIL FERTILITY IN WUKARI URBAN AREA, TARABA STATE, NIGERIA. *Journal of Science Research and Reviews*. https://doi.org/10.70882/josrar.2026.v3i6.249

INTRODUCTION

Soil fertility is a fundamental determinant of agricultural productivity and ecosystem sustainability, particularly in rapidly expanding urban and peri-urban environments

This work is licensed under the Creative Commons Attribution 4.0 International License

where land use pressures intensify soil degradation processes (Keshavarzi *et al.*, 2025; Özyazici *et al.*, 2017; Sharma *et al.*, 2020). Traditional assessments of soil fertility have largely relied on point-based and univariate analyses, which often fail to capture the inherent spatial heterogeneity measurements and multivariate interactions governing nutrient availability. However, soil properties are intrinsically spatially structured, influenced by both natural pedogenic processes and anthropogenic activities, necessitating analytical approaches that explicitly account for spatial dependence and multivariate complexity (Keshavarzi *et al.*, 2025; Kila & Ragasan, 2026).

Geostatistics provides a robust framework for quantifying spatial variability through the theory of regionalized variables, enabling the characterization of spatial dependence using semivariograms and the prediction of unsampled locations via kriging (Alshahrani *et al.*, 2025; Sharma *et al.*, 2020). Concurrently, multivariate statistical techniques such as Principal Component Analysis allow for the reduction of dimensional complexity and the identification of dominant fertility gradients from correlated soil properties (Parvizi & Fatehi, 2025; Shokr *et al.*, 2025; Zeraatpisheh *et al.*, 2025). The integration of these approaches has emerged as a powerful strategy for soil fertility assessment, facilitating the development of composite indices that reflect underlying soil chemical structure while preserving spatial continuity (Marchetti *et al.*, 2012; Ramzan *et al.*, 2017; Shokr *et al.*, 2025; Singh, 2026).

Despite these advances, many soil fertility studies continue to rely on arbitrary weighting schemes or independent interpolation of individual nutrients, thereby neglecting the structural interdependencies among soil variables. In particular, the role of exchange-complex chemistry—comprising exchangeable bases, cation exchange capacity, and base saturation—in defining large-scale fertility gradients remains underexplored within integrated geostatistical frameworks. Furthermore, limited attention has been given to evaluating the robustness of fertility indices to variable selection and to assessing the scale-dependent nature of spatial heterogeneity in urban soil systems (Özyazici *et al.*, 2017; Sharma *et al.*, 2020; Venkateswarlu *et al.*, 2025).

Urban soils are especially characterized by high spatial variability due to mixed land use, anthropogenic disturbances, and localized management practices, resulting in complex and patchy fertility patterns (Kila & Ragasan, 2026; Parvizi & Fatehi, 2025). The Wukari urban area in northeastern Nigeria presents a relevant case for such investigation due to its heterogeneous land use patterns and evolving soil management practices. Understanding the spatial structure of soil fertility in this context is essential for targeted land management and sustainable urban agriculture. This study therefore aims to characterize the multivariate structure of soil fertility using PCA, develop a data-driven Soil Fertility Index based on dominant fertility gradients, quantify spatial dependence through variogram modeling, generate continuous fertility surfaces using ordinary kriging, and evaluate model performance and index robustness using cross-validation and sensitivity analysis.

MATERIALS AND METHOD

Study area and sampling design.

A total of 70 soil samples were collected across the Wukari urban area using a spatially distributed sampling approach designed to capture intra-urban variability. Geographic coordinates were recorded in the field using a handheld GPS receiver and referenced to the WGS 1984 datum. For spatial analysis, all coordinates were projected to Universal Transverse Mercator Zone 32N to ensure Euclidean distance consistency for semivariogram estimation and kriging (Keshavarzi *et al.*, 2025; Singh, 2026; Zeraatpisheh *et al.*, 2025). Although 70 locations were initially sampled, following quality control screening, 50 locations containing complete macro–exchange datasets and valid projected coordinates were retained for multivariate and geostatistical analysis.

Laboratory determinations.

Laboratory analyses were conducted to quantify macro–exchange indicators representing structural soil fertility. These included soil reaction (pH), electrical conductivity, particle size fractions (sand, silt, clay), bulk density, particle density, porosity, organic carbon, organic matter, total nitrogen, available phosphorus, exchangeable bases (Ca, Mg, K, Na), total exchangeable bases, total exchangeable acidity, effective cation exchange capacity, percent base saturation, sodium adsorption ratio, and exchangeable sodium percentage. These parameters collectively characterize the exchange complex, nutrient retention capacity, ionic balance, and structural stability of soils (Kila & Ragasan, 2026; Marchetti *et al.*, 2012; Özyazici *et al.*, 2017; Parvizi & Fatehi, 2025; Ramzan *et al.*, 2017; Sharma et al., 2020; Venkateswarlu *et al.*, 2025). The focus on macro–exchange variables reflects the study's objective to model structural fertility gradients rather than trace-element variability. Micronutrients (Zn, Fe, Cu, Mn) were excluded from this phase to avoid conflating exchange-complex fertility with trace-element geochemistry.

Data processing and statistical analysis.

Raw laboratory outputs were initially compiled in Microsoft Excel prior to statistical processing. Quality control screening was conducted to ensure analytical and spatial completeness. Observations lacking valid coordinate pairs or containing incomplete macro–exchange measurements were excluded without imputation. Data were imported into R (v4.3.2) for harmonization and verification. Variable names were standardized, measurement units were

checked for consistency, and coordinate projections were confirmed in UTM Zone 32N. A structured project directory was established separating raw data, cleaned datasets, tabular outputs, raster outputs, and figures to ensure computational reproducibility.

Exploratory data analysis.

For each variable, the mean, standard deviation, coefficient of variation, skewness, and kurtosis were computed. The coefficient of variation was used to quantify relative variability and assess the magnitude of spatial heterogeneity. Skewness and kurtosis were examined to evaluate deviation from symmetry and normality. Although selected exchange-related variables exhibited moderate to high skewness, overall dispersion patterns were internally coherent and consistent with environmental soil data. No transformation procedures were applied, as distributional characteristics did not compromise principal component extraction or violate assumptions underlying intrinsic stationarity. Pearson's correlation coefficients were computed to evaluate linear associations among macro–exchange variables and to detect structural redundancy prior to dimensional reduction.

Principal component analysis and Soil Fertility Index derivation.

Principal component analysis was applied to the standardized macro–exchange dataset to identify orthogonal latent dimensions governing fertility structure (Ayodotun *et al.*, 2019; Kila & Ragasan, 2026). Standardization to zero mean and unit variance was performed to remove scale effects and ensure equal contribution of variables to covariance estimation. The first principal component, associated with the largest eigenvalue, explained the greatest proportion of total variance and was interpreted as the dominant fertility gradient. The Soil Fertility Index was computed directly from the first principal component scores as a linear combination of standardized macro–exchange variables weighted by their corresponding eigenvector coefficients. In this formulation, the weights are not arbitrarily assigned but are derived from the eigenstructure of the covariance matrix, reflecting each variable's contribution to the dominant variance direction. Because PC1 maximizes total explained variance subject to orthogonality constraints, the resulting SFI represents the dominant latent fertility gradient embedded in the macro–exchange system, free from subjective weighting bias.

Sensitivity analysis.

To evaluate structural robustness of the derived SFI, a leave-one-variable-out sensitivity analysis was conducted. PCA was iteratively recomputed after sequential exclusion of each macro–exchange variable. For each iteration, the resulting PC1 scores were correlated with the baseline SFI derived from the full variable set. High correlation values indicate structural resilience of the fertility gradient to exclusion of individual variables, whereas substantial declines suggest dependency on specific components (I. K, 2023; Kila & Ragasan, 2026; Singh, 2026). This procedure provided a quantitative measure of index stability and verified that the dominant fertility structure was not driven by isolated variables but by coherent exchange-complex clustering.

Spatial dependence modeling.

Spatial autocorrelation was quantified using the experimental semivariogram. Spatial modeling was conducted within the framework of intrinsic stationarity, whereby the mean of the regionalized variable is assumed locally constant and spatial dependence is expressed through the semivariogram as a function of separation distance only. Isotropy was assumed, as exploratory diagnostics did not indicate systematic anisotropy at the spatial scale of sampling. Lag intervals were defined to ensure sufficient pair counts within each distance class while preserving sensitivity to short-range spatial structure. Theoretical semivariogram models (spherical, exponential, Gaussian, and stable) were fitted using weighted least squares optimization. For each variable, model parameters—nugget, partial sill, and range—were estimated by minimizing the residual sum of squares between experimental and theoretical semivariance values (An *et al.*, 2022; Özen, 2019). Model selection was based on the minimum residual sum of squares criterion, ensuring objective determination of the best-fitting structure. Spatial dependence strength was evaluated using the nugget-to-sill ratio expressed as a percentage, where lower values indicate stronger spatial dependence (Keshavarzi et al., 2025; Kila & Ragasan, 2026; Ramzan *et al.*, 2017; Sharma *et al.*, 2020; Shokr *et al.*, 2025).

Spatial prediction and validation.

Spatial prediction was performed using ordinary kriging, a best linear unbiased estimator appropriate for environmental variables exhibiting spatial dependence with an unknown but locally constant mean. Unlike deterministic interpolation methods, ordinary kriging explicitly incorporates the fitted semivariogram model to account for spatial autocorrelation and to quantify prediction uncertainty (Kila & Ragasan, 2026; Marchetti *et al.*, 2012; Yakub *et al.*, 2022). Prediction was performed on a regular grid with 50 m spatial resolution, and kriging outputs were clipped to the administrative boundary of the Wukari urban area to prevent extrapolation beyond the spatial support of the sampled domain. Predictive performance was evaluated using leave-one-out cross-validation, yielding mean error (unbiasedness), root mean square error (accuracy), and root mean square standardized error (uncertainty calibration). Global

Moran's I was computed to evaluate large-scale spatial organization beyond the local dependence captured by the semivariogram, providing a global measure of spatial autocorrelation across the study area.

Spatial classification.

To facilitate spatial interpretation, the continuous SFI surface was classified using a standard deviation–based scheme. Classification thresholds were defined relative to the mean and standard deviation of the SFI distribution: Very Low (below mean minus one standard deviation), Low (mean minus one standard deviation to mean), Moderate (mean to mean plus one standard deviation), High (mean plus one to two standard deviations), and Very High (above mean plus two standard deviations). This approach was selected to provide relative differentiation of fertility conditions based on the statistical distribution of the derived index rather than externally imposed agronomic thresholds. The spatial extent of each fertility class was quantified by computing raster cell frequencies and converting cell counts to hectares.

RESULTS AND DISCUSSION

Results

Table 1: Descriptive Statistics of Soil Physicochemical Properties

Variable	Minimum	Maximum	Range	Mean	SD	CV (%)	Skewness	Kurtosis
pH	5.3	7.29	1.99	6.2558	0.497197	7.94777	0.100311	-0.73061
EC	0.03	0.63	0.6	0.07572	0.086931	114.8057	5.232823	30.14733
Sand (%)	68	87.2	19.2	79.61	5.02643	6.313818	-0.52745	-0.38378
Silt (%)	6.8	20.2	13.4	10.994	3.277219	29.80916	1.039775	0.578259
Clay (%)	4.2	16.2	12	9.396	3.294892	35.06696	0.487666	-0.98729
BD (g/cm^3)	1.49	1.73	0.24	1.6046	0.05946	3.705628	-0.10756	-0.96403
PD (g/cm^3)	2.09	2.93	0.84	2.510667	0.213612	8.508164	-0.3016	-0.77766
POROSITY	27.61	41.125	13.515	35.7821	3.906671	10.91795	-0.62505	-0.84217
OC (g/kg)	4.9875	14.49638	9.508875	10.88597	2.423164	22.2595	-0.93598	0.074018
OM (g/kg)	8.59845	24.99175	16.3933	18.76741	4.177533	22.25951	-0.93598	0.074016
TN (g/kg)	0.39875	2.499	2.10025	1.708996	0.462076	27.03786	-0.65806	-0.18164
AVP (mg/kg)	6.4603	19.1	12.6397	11.83949	2.824873	23.85976	0.674231	0.218
Ca (cmol/kg)	0.4	27.5992	27.1992	3.559134	3.796194	106.6606	5.032769	29.22035
Mg (cmol/kg)	1.0299	3.913621	2.883721	2.016724	0.850514	42.17302	0.716582	-0.75058
K (cmol/kg)	0.25641	1.487179	1.230769	0.908513	0.216697	23.85179	0.147753	1.252533
Na (cmol/kg)	0.086957	3.695652	3.608696	0.712174	0.654618	91.91824	2.327136	6.789907
TEB (cmol/kg	4.41937	31.6986	27.27923	8.013221	3.644727	45.48393	5.442107	32.72581
TEA (cmol/kg)	1.2	3.76	2.56	2.1426	0.708404	33.06281	0.532718	-0.71461
ECEC (cmol/kg)	5.82937	35.1586	29.32923	10.0773	3.966595	39.36169	5.02407	29.06076
PBS (%)	61.70028	90.15888	28.4586	76.4822	5.418645	7.084845	-0.14697	0.22317
SAR	0.058102	2.261221	2.203119	0.437304	0.392697	89.79951	2.431791	7.518217
ESP (%)	0.991193	27.79655	26.80535	8.063053	5.442636	67.50093	1.301256	1.887468

The descriptive statistical profile reveals a chemically structured system characterized by pronounced heterogeneity in exchange-complex dynamics and localized nutrient imbalances. Soil reaction ranged from moderately acidic to near-neutral (mean 6.26, CV=7.95%), exhibiting low dispersion and near-symmetric distribution. The relative homogeneity of pH suggests a broadly stable biochemical environment. In contrast, electrical conductivity demonstrated extreme variability (CV=114.81%) and strong positive skewness (5.23), accompanied by pronounced leptokurtosis (30.15), indicating discrete salinity hotspots rather than uniform salinity influence.

The soils are dominantly sandy (mean sand 79.61%, CV=6.31%), while silt and clay contents show moderate dispersion (CV≈30–35%). Bulk density, particle density, and porosity exhibited low to moderate variability (CV=3.7–10.9%) and near-normal distributions, suggesting structural stability and minimal mechanical constraints to root growth or water movement. The relative homogeneity of physical properties implies that fertility variability is unlikely to be structurally or texturally controlled. Instead, the observed differentiation must originate from chemical processes within the exchange complex.

Organic carbon and organic matter displayed identical statistical behavior (CV≈22.26%), reflecting their direct conversion relationship. Total nitrogen exhibited comparable dispersion (CV=27.04%), reinforcing a relatively consistent organic–nitrogen coupling throughout the study area. The moderate variability in the C:N ratio (CV=24.35%) further supports the inference of relatively stable organic nutrient cycling.

Table 2: Nutrient Ratio Statistics

Variable	Mean	SD	CV%
NP_ratio	0.152754	0.055571	36.37921
NK_ratio	2.051436	1.012622	49.3616
PK_ratio	14.04177	5.64862	40.22725
CaMg_ratio	2.061882	2.097343	101.7199
CN_ratio	6.629875	1.61428	24.34858
Base_Acid_ratio	3.987186	1.453823	36.46238

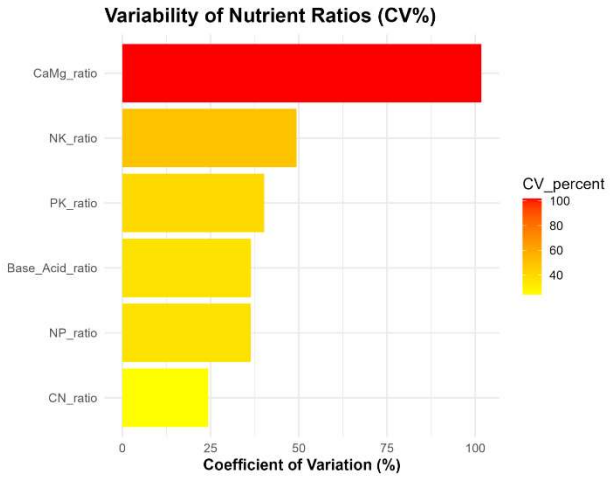


Figure 1: Variability of nutrient ratio

The most striking feature lies in the behavior of exchangeable calcium, which exhibited exceptionally high variability (CV=106.66%), coupled with strong positive skewness (5.03) and leptokurtosis (29.22). This statistical profile indicates highly localized enrichment zones that substantially exceed background levels. Total exchangeable bases and effective cation exchange capacity also showed substantial variability (CV=45.48% and 39.36%, respectively), suggesting that the exchange complex is chemically heterogeneous across the landscape. Magnesium displayed moderate variability (CV=42.17%), whereas potassium remained comparatively stable (CV=23.85%). Sodium-related indicators (Na, SAR, ESP) exhibited high coefficients of variation (67–92%) and positive skewness, revealing localized sodicity-prone environments. The Ca:Mg ratio exhibited extreme variability (CV=101.72%), underscoring pronounced cation imbalance across sampling locations. Despite variability in absolute cation concentrations, percent base saturation remained relatively stable (CV=7.08%), indicating consistent proportional dominance of base cations across the landscape. This apparent paradox—high variability in cation magnitude but stability in base proportion—suggests that fertility differentiation is driven more by total exchangeable capacity than by shifts in base–acid equilibrium.

Table 3: Macronutrient Correlation Matrix

	TN_pct	AVP	K	Ca	Mg	Na	OM	OC_pct	TEB	TEA	ECEC	PBS
TN_pct	1.000	-0.090	-0.127	0.320	0.070	0.125	0.787	0.787	0.227	0.148	0.235	0.274
AVP	-0.090	1.000	-0.067	-0.133	-0.290	-0.098	0.190	0.190	-0.030	-0.239	-0.091	-0.062
K	-0.127	-0.067	1.000	-0.225	0.066	0.069	-0.047	-0.047	-0.118	-0.181	-0.146	0.192
Ca	0.320	-0.133	-0.225	1.000	-0.034	0.234	0.133	0.133	0.930	0.436	0.950	0.422
Mg	0.070	-0.290	0.066	-0.034	1.000	-0.010	-0.157	-0.157	0.061	0.256	0.115	0.044
Na	0.125	-0.098	0.069	0.234	-0.010	1.000	-0.071	-0.071	0.309	0.376	0.357	0.131
OM	0.787	0.190	-0.047	0.133	-0.157	-0.071	1.000	1.000	0.155	-0.200	0.097	0.246
OC_pct	0.787	0.190	-0.047	0.133	-0.157	-0.071	1.000	1.000	0.155	-0.200	0.097	0.246
TEB	0.227	-0.030	-0.118	0.930	0.061	0.309	0.155	0.155	1.000	0.358	0.971	0.422
TEA	0.148	-0.239	-0.181	0.436	0.256	0.376	-0.200	-0.200	0.358	1.000	0.526	-0.391
ECEC	0.235	-0.091	-0.146	0.950	0.115	0.357	0.097	0.097	0.971	0.526	1.000	0.358
PBS	0.274	-0.062	0.192	0.422	0.044	0.131	0.246	0.246	0.422	-0.391	0.358	1.000

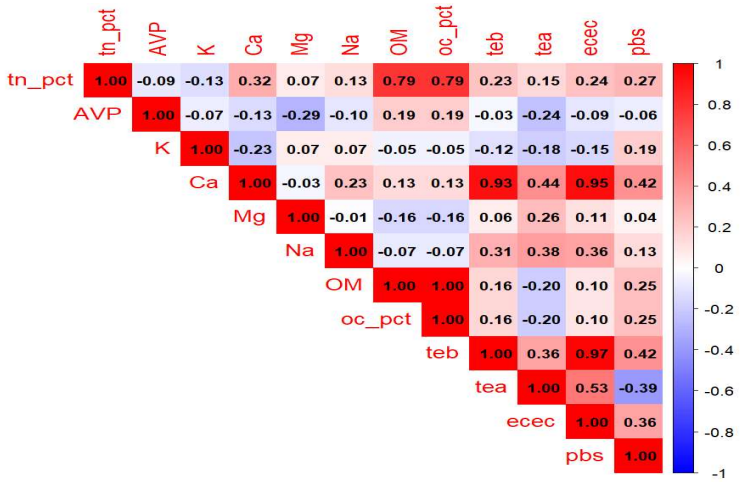


Figure 2: Macronutrient Correlation Heatmap

The correlation matrix demonstrates the emergence of a dominant cationic cluster centered on exchangeable calcium. Calcium exhibited extremely strong positive correlations with total exchangeable bases (r=0.93) and effective cation exchange capacity (r=0.95), while TEB and ECEC were almost perfectly correlated (r=0.97). This triadic relationship confirms that the exchange complex in the study area is structurally Ca-dominated, with calcium exerting disproportionate influence on total exchange capacity. The magnitude of these correlations indicates substantial multicollinearity among exchange-complex indicators. Organic matter and total nitrogen were strongly correlated (r=0.79), reflecting tight organic–nitrogen coupling. In contrast, available phosphorus demonstrated weak correlations with most exchangeable bases and organic indicators (r<0.30), indicating that phosphorus dynamics are relatively independent of the exchange complex. Potassium exhibited weak to moderate relationships and did not integrate strongly into the dominant Ca–exchange complex cluster. Sodium showed moderate correlations with TEB (r=0.31) and ECEC (r=0.36), indicating partial alignment with exchange magnitude but not structural dominance.

Table 4: PCA eigenvalues and variance explained

Component	Eigenvalue	Variance Percent	Cumulative Variance
1	3.787299054	31.56082545	31.56082545
2	2.743321394	22.86101161	54.42183706
3	1.424145644	11.86788036	66.28971743
4	1.339374873	11.16145728	77.4511747
5	0.990399082	8.253325687	85.70450039
6	0.747682007	6.230683393	91.93518378
7	0.628349204	5.236243367	97.17142715
8	0.242778586	2.023154887	99.19458204
9	0.079908601	0.665905009	99.86048705
10	0.01389782	0.115815169	99.97630221
11	0.002843734	0.023697785	100
12	5.57E-11	4.64E-10	100

Table 5: PC Loadings

	Dim.1	Dim.2	Dim.3	Dim.4	Dim.5
TN_pct	0.609066	0.562932	-0.32597	0.319312	0.065317
AVP	-0.09872	0.339086	0.06714	-0.66715	0.151495
K	-0.18111	0.045794	0.55218	0.436246	0.43117
Ca	0.903426	-0.27218	0.101535	-0.18549	-0.15784
Mg	0.05855	-0.29281	-0.12254	0.681764	-0.33217
Na	0.369585	-0.31505	0.01758	0.089308	0.750602
OM	0.457845	0.850752	-0.16987	0.072086	0.056727
OC_pct	0.457844	0.850753	-0.16987	0.072089	0.056725

TEB	0.891394	-0.26749	0.195055	-0.17521	-0.08625
TEA	0.400667	-0.59168	-0.58496	0.084702	0.202643
ECEC	0.901431	-0.36569	0.086635	-0.12679	-0.05465
PBS	0.480264	0.217604	0.733082	0.174598	-0.14387

Principal component analysis further clarifies the hierarchical structure. The first principal component accounted for 31.56% of total variance, while the first four components collectively explained 77.45%, indicating that soil fertility dynamics are multidimensional but structured within a limited number of dominant gradients. PC1 was strongly and positively loaded by calcium (0.903), ECEC (0.901), and TEB (0.891), confirming the statistical dominance of the exchange complex. Total nitrogen (0.609), organic matter (0.458), organic carbon (0.458), percent base saturation (0.480), and sodium (0.370) also contributed positively to this axis. PC1 represents an exchange-complex enrichment gradient, integrating both cation reserve capacity and organic nutrient status. Notably, available phosphorus and potassium exhibited negligible contributions to PC1. Thus, the Soil Fertility Index derived from PC1 fundamentally reflects exchange-complex magnitude and associated nutrient enrichment rather than balanced NPK dynamics.

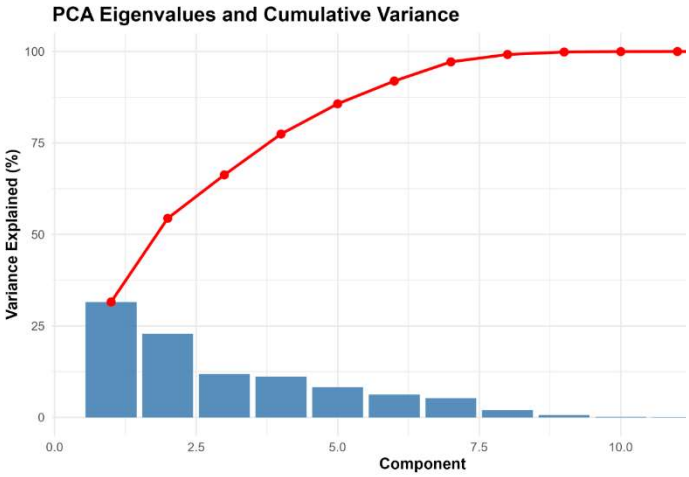


Figure 3: Eigenvalues and cumulative variance

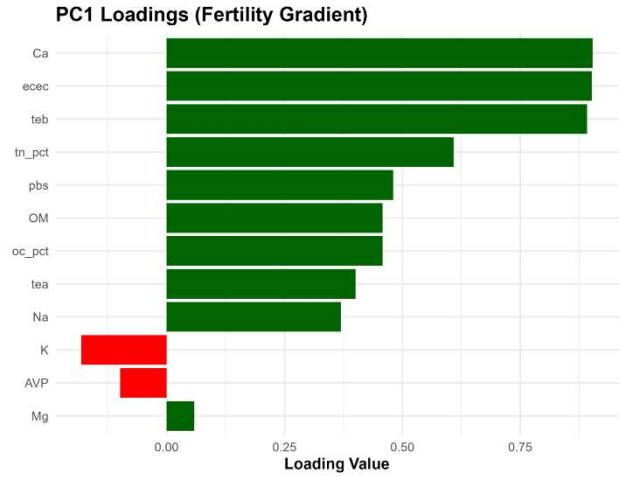
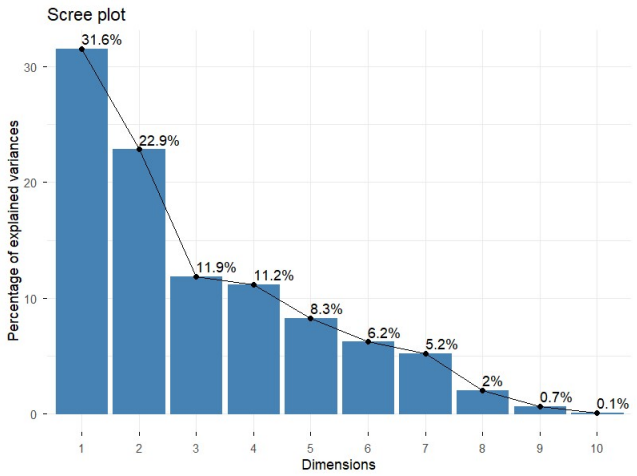


Figure 4: PC1 Loadings

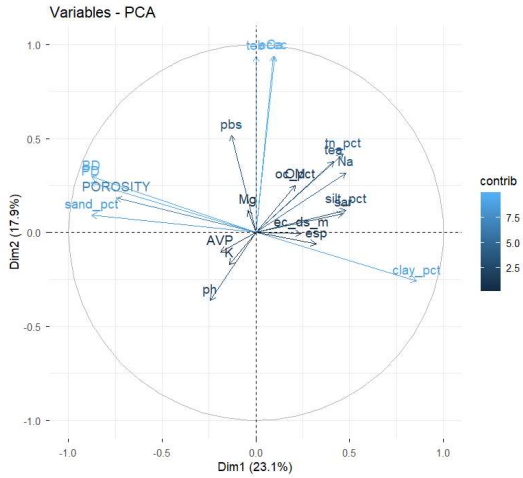
The second principal component (22.86% variance explained) was characterized by strong positive loadings for organic matter (0.851) and organic carbon (0.851), coupled with a moderate negative loading for exchangeable acidity (−0.592), capturing variability in organic enrichment relative to acidity status. PC3 (11.87%) exhibited strong positive loading for percent base saturation (0.733) and moderate loading for potassium (0.552), indicating a base-saturation–potassium gradient. PC4 (11.16%) was characterized by high loading of magnesium (0.682) and moderate contributions from potassium and nitrogen, reflecting secondary cation balance adjustments.

Table 6: SFI Sensitivity Analysis

Removed Variable	Correlation with Baseline SFI
TN_pct	0.958857221
AVP	0.999459963
K	0.998744899
Ca	0.885944851
Mg	0.999824278
Na	0.992536662
OM	0.97371688
OC_pct	0.973716954
TEB	0.896921299
TEA	0.984823155
ECEC	0.86716437
PBS	0.988042819



Figures 5: Scree plot and variable contributions



Figures 6: Scree plot and variable contributions

Sensitivity analysis of the PCA-derived Soil Fertility Index provides critical methodological insight. Removal of exchange-complex variables substantially altered the SFI structure, with the largest declines in correlation observed when ECEC (r=0.867), calcium (r=0.886), or TEB (r=0.897) were excluded. In contrast, removal of available phosphorus (r=0.999), potassium (r=0.999), or magnesium (r=0.9998) produced negligible changes. This asymmetry confirms that the SFI is structurally dependent on exchange-complex magnitude, whereas phosphorus and potassium contribute minimally to the dominant fertility gradient. The stability of the index under removal of organic variables (OM, TN; r≈0.96–0.97) further suggests that exchange-complex chemistry exerts primary control over multivariate fertility differentiation.

Table 7: Variogram Parameters for all Variables

Variable	Nugget	Sill	Range (m)	Nugget to Sill Ratio (%)
pH	0.229661097	0.441725931	27992.76717	51.9917626
EC_ds_m	0	0.012971698	11348.17777	0
sand_pct	18.41108898	3583.793413	2794762.117	0.513731872
silt_pct	11.12958946	11.17797071	9559.383979	99.56717319
clay_pct	10.28854677	20.5498791	36355.35235	50.06621556
BD	0.0032534	0.014144703	53323.16967	23.00083527
PD	0.044805773	0.065524002	28037.48347	68.38070255
POROSITY	16.00628729	16.65959624	17936.04386	96.07848267
OC_pct	5.701623925	6.241177738	10011.55167	91.35493596
OM	16.9458032	18.55024059	10013.85448	91.35085405
TN_pct	0	0.216637269	930.7486597	0
AVP	0	7.839020382	1306.213271	0
Ca	12.66214966	16.39362024	3768.821721	77.23827608
Mg	0.741113	0.749006197	665.2785369	98.94617736
K	0.045702836	0.049216285	14020.31927	92.86120573
Na	0	0.390249854	1838.706361	0
TEB	12.28025599	16.03616868	3637.565333	76.57849098
TEA	0	0.487962237	382.2585088	0
ECEC	14.33936903	18.59145953	3620.591224	77.12879674
PBS	23.65089574	31.10722862	767.3499731	76.03022444
SAR	0	0.145379841	1931.894177	0
ESP	0	29.56673526	1501.788478	0

Semivariogram analysis revealed variable degrees of spatial dependence among soil properties, with nugget-to-sill ratios ranging from 0% to 99.6%. Total nitrogen, available phosphorus, sodium, exchangeable acidity, SAR, and ESP exhibited negligible nugget effects relative to total sill (NSR=0%), indicating strong spatial structure. The effective ranges for these properties were relatively short (TN≈931 m; AVP≈1306 m), implying that their spatial

influence is localized but predictable within neighborhood scales. Exchangeable calcium (77.24%), TEB (76.58%), ECEC (77.13%), pH (51.99%), and clay (50.07%) exhibited moderate spatial dependence. The exchange-complex variables showed effective ranges between approximately 3.6 and 3.8 km, suggesting broader-scale spatial structuring compared to TN or AVP, potentially reflecting parent material influence or systematic management patterns. Organic matter (91.35%), organic carbon (91.35%), magnesium (98.95%), potassium (92.86%), silt (99.57%), and porosity (96.08%) exhibited weak spatial dependence characterized by high nugget effects, indicating strong short-distance variability and reduced spatial predictability.

The PCA-derived Soil Fertility Index exhibited a nugget-to-sill ratio of 76.08% under a Stable variogram model, indicating weak to moderate spatial dependence. The effective range of approximately 17.6 km suggests that fertility gradients extend across substantial portions of the study area, albeit with considerable micro-scale variability. The relatively high nugget proportion confirms that localized heterogeneity contributes significantly to fertility differentiation. The adoption of a Stable model implies gradual decay in spatial autocorrelation rather than abrupt cutoffs, reflecting smooth transitions in fertility conditions across space.

Table 8: Global Moran's I statistics

Variable	Moran I	Expected I	P value
TN_pct	0.046824	-0.02041	0.227769
AVP	0.030413	-0.02041	0.285468
K	-0.02147	-0.02041	0.504787
Ca	0.011809	-0.02041	0.265629
Mg	-0.07739	-0.02041	0.735123
Na	-0.01201	-0.02041	0.459494

Global Moran's I statistics for key fertility indicators were generally low (−0.08 to 0.05) and statistically non-significant ($p>0.22$), indicating the absence of strong global clustering patterns. While this may appear inconsistent with variogram-detected spatial structure, these metrics capture different spatial dimensions: variograms quantify spatial dependence across distance lags, while Moran's I evaluates overall clustering across the entire study domain. The combination of moderate variogram structure and weak global Moran's I suggests that fertility heterogeneity is spatially patchy rather than regionally aggregated, consistent with urban soil systems where anthropogenic inputs and land-use heterogeneity generate spatial mosaics.

Table 9: Cross-validation Summary

Variable	Mean Error	RMSE	Mean Std Error	RMSS
pH	-0.002645821	0.502065005	-0.002679637	1.017882
ec_ds_m	0.001908884	0.092966864	0.013062427	1.213248
sand_pct	0.004782413	4.900486152	0.000498929	1.01392
silt_pct	0.000170799	3.305912058	2.53E-05	0.979893
clay_pct	-0.00577844	3.208309134	-0.000878486	0.975989
BD	0.000100078	0.057671802	0.000853968	0.984391
PD	0.00012166	0.210240073	0.000282557	0.970711
POROSITY	0.000387314	3.920896705	4.78E-05	0.963328
oc_pct	-0.001692458	2.438848529	-0.000339537	0.978329
OM	-0.002919209	4.204569195	-0.000339701	0.978327
tn_pct	0.000206463	0.469662879	0.000224376	1.006537
AVP	0.015550991	2.813645441	0.002889638	1.01913
Ca	0.00128714	3.80057943	0.000158478	0.936222
Mg	8.02E-07	0.859226506	4.58E-07	0.982844
K	5.43E-05	0.217108936	0.000124068	0.992641
Na	0.013194307	0.735096453	0.01121342	1.320205
Teb	6.23E-06	3.702541693	7.91E-07	0.922163
Tea	-5.70E-07	0.715667079	-4.04E-07	1.014219
Ecec	0.000509962	4.008604608	5.89E-05	0.927025
Pbs	0.000518401	5.484473437	4.60E-05	0.974047
Sar	0.007096326	0.500651766	0.009613258	1.583322

Esp	0.028206104	6.090547253	0.002594781	1.17793

Cross-validation diagnostics demonstrate strong predictive performance of the kriging models. Mean prediction errors for all variables were effectively zero (ME<0.03), indicating unbiased estimations. Root Mean Square Standardized values were generally close to unity for most properties (0.92–1.02), confirming reliable uncertainty estimation. Variables exhibiting high skewness and extreme dispersion, such as SAR (RMSS=1.58) and Na (RMSS=1.32), showed slight underestimation of variability, which is expected for highly asymmetric distributions and does not undermine overall model robustness. Exchange-complex variables displayed RMSS values slightly below 1 (≈0.92–0.94), indicating mild overestimation of uncertainty but remaining within acceptable calibration limits.

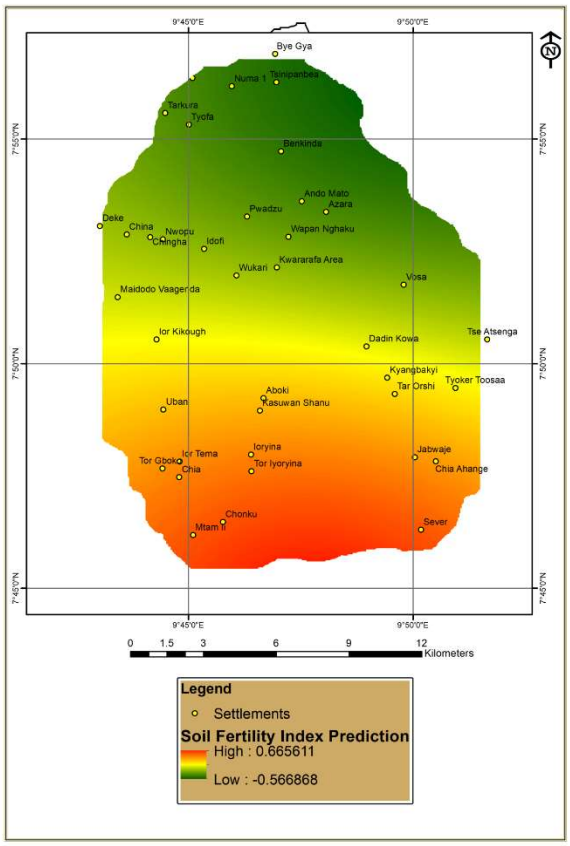


Figure 7: Soil Fertility Index Map of Wukari

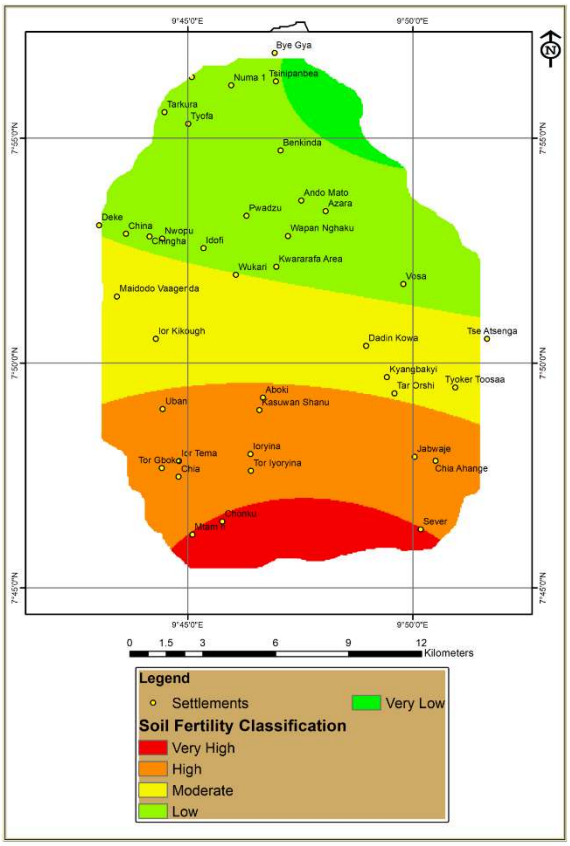


Figure 8: Soil Fertility Classification in Wukari and Environs

Table 10: SFI Class Area Summary

Class	Pixel_Count	Area_m2	Area_ha	Class_Label
1	3539	8847500	884.75	Very Low
2	36494	91235000	9123.5	Low
3	28345	70862500	7086.25	Moderate
4	28988	72470000	7247	High
5	8291	20727500	2072.75	Very High

The spatial classification of the PCA-derived Soil Fertility Index reveals a heterogeneous but structured fertility landscape. Using a standard deviation–based classification approach, the total mapped area covered approximately 26,414 ha. The proportional distribution was: Very Low 884.75 ha (3.35%), Low 9,123.50 ha (34.54%), Moderate 7,086.25 ha (26.82%), High 7,247.00 ha (27.44%), and Very High 2,072.75 ha (7.85%). Notably, moderate-to-high fertility zones collectively account for 54.26% of the study area, indicating that more than half of the landscape exhibits structurally favorable chemical fertility conditions. In contrast, severely constrained zones (Very Low fertility) represent only 3.35% of the total area,

suggesting that extreme nutrient limitation is spatially restricted.

The spatial configuration of fertility classes reflects a mosaic structure rather than large, contiguous fertility blocks. Moderate and High fertility zones are interspersed across the landscape, consistent with the weak global Moran's I results and moderate SFI nugget-to-sill ratio. Low fertility zones, occupying over one-third of the area, appear spatially distributed rather than concentrated in a single region. Very High fertility zones (7.85%) are spatially limited and likely correspond to areas of elevated exchange capacity and calcium enrichment. Given that PC1 (SFI) is strongly loaded by calcium, ECEC, and TEB, the spatial distribution of fertility classes primarily reflects variation in exchange-complex magnitude rather than balanced NPK status. Areas classified as High or Very High fertility correspond to zones of elevated exchangeable Ca and overall cation reserve capacity. The limited influence of available phosphorus and potassium in defining PC1 implies that SFI zoning is not driven by simple macronutrient abundance but by structural chemical buffering capacity.

Discussion

The multivariate and geostatistical analyses collectively demonstrate that soil fertility differentiation in the Wukari urban area is fundamentally governed by exchange-complex chemistry, particularly calcium dominance and associated cation reserve capacity. The strong loadings of Ca, ECEC, and TEB on PC1 (0.90–0.90), coupled with near-perfect correlations among these variables (r=0.93–0.97), indicate that fertility gradients are structurally anchored in exchangeable base magnitude rather than balanced macronutrient dynamics. This chemical architecture suggests that spatial fertility differentiation is controlled more by the quantity and buffering capacity of exchange sites than by simple nutrient concentration variability (Venkateswarlu *et al*., 2025). Areas classified as high SFI are therefore not merely nutrient-rich but chemically resilient due to elevated cation exchange capacity and dominant base saturation. The pronounced variability and positive skewness observed for exchangeable Ca (CV=106.66%; skewness=5.03) further indicate localized enrichment processes, which may reflect parent material heterogeneity, differential weathering intensity, or spatially uneven anthropogenic inputs common within urban landscapes. The co-dominance of Ca, TEB, and ECEC implies that calcium availability exerts disproportionate influence on overall fertility potential.

In contrast, available phosphorus exhibited weak correlations with exchange-complex variables and minimal influence on PC1. This relative independence suggests that phosphorus dynamics are governed by fixation–release processes distinct from exchange capacity control. Consequently, the fertility system in the study area cannot be described as a simple NPK-driven regime; rather, it is a chemically buffered, exchange-dominated system with layered nutrient adjustments (Marchetti *et al.*, 2012; Özen, 2019; Özyazici et al., 2017; Ramzan *et al.*, 2017; Sharma *et al*., 2020; Singh, 2026).

Although variogram modeling revealed measurable spatial structure for exchange-complex variables (moderate nugget-to-sill ratios ≈76–77%), global Moran's I statistics indicated weak overall clustering. This apparent contrast highlights the scale-dependent nature of spatial fertility patterns. Variograms detect spatial dependence across specific lag distances, whereas Moran's I measures global clustering across the entire domain. The coexistence of moderate variogram structure and weak global autocorrelation indicates that fertility heterogeneity operates primarily at localized scales, producing a mosaic of enrichment and depletion patches rather than broad, contiguous fertility zones. The SFI variogram range (≈17.6 km) suggests that fertility gradients extend across substantial portions of the landscape; however, the high nugget proportion (76.08%) confirms the presence of significant micro-scale variability. This spatial configuration is characteristic of urban and peri-urban soils, where land-use variability, localized organic inputs, construction activities, and anthropogenic disturbances generate patch-level chemical differentiation (Kila & Ragasan, 2026). Fertility heterogeneity in the Wukari urban area is therefore spatially structured but fragmented, reinforcing the need for site-specific nutrient management rather than blanket fertilization strategies.

The extreme variability of the Ca:Mg ratio (CV=101.72%) and high dispersion of sodium-related indicators (CV up to 91.92%) reveal localized cation imbalance zones within the broader fertility framework. While percent base saturation remained relatively stable (CV=7.08%), the magnitude of exchangeable bases varied substantially, indicating that proportional dominance does not necessarily reflect balanced cation dynamics. High Ca-dominated zones, while chemically enriched, may influence nutrient uptake interactions, particularly with Mg and K. Conversely, areas exhibiting elevated Na, SAR, or ESP may face structural risks under irrigation or intensive cultivation, despite otherwise moderate fertility classification. The spatial dominance of Moderate and High SFI classes (54.26% combined) suggests considerable intrinsic fertility potential across much of the study area. However, the substantial Low fertility coverage (34.54%) indicates that targeted nutrient augmentation or organic amendment may be required in over one-third of the landscape. Importantly, fertility classification reflects exchange-complex strength rather than direct crop yield prediction.

The sensitivity analysis of the Soil Fertility Index provides a notable methodological contribution. The substantial decline in SFI stability when Ca, ECEC, or TEB were removed (correlations dropping to 0.867–0.897) confirms

that the index is structurally anchored in exchange-complex dynamics. Conversely, the negligible impact of removing AVP or K (correlations ≈0.999) demonstrates that the dominant fertility gradient is not driven by isolated macronutrient variability. This robustness analysis strengthens confidence in the PCA-derived index and demonstrates that SFI is not an arbitrary aggregation of variables but a statistically coherent fertility construct. Furthermore, the integration of descriptive statistics, correlation analysis, PCA, variogram modeling, Moran's I diagnostics, cross-validation, and spatial classification represents a comprehensive systems-based approach to fertility evaluation. Rather than mapping individual nutrients in isolation, the study quantifies the hierarchical structure of fertility drivers and their spatial expression.

The findings underscore the importance of integrating multivariate analysis with geostatistical modeling in urban soil studies. The chemically structured yet spatially patchy fertility system observed in Wukari urban soils illustrates how exchange-complex dominance and localized anthropogenic influences can coexist within a single landscape. This integrated methodological framework enables identification of structural fertility drivers, spatial continuity patterns, fertility class dominance, management-priority zones, and model reliability and uncertainty, offering a replicable model for fertility assessment in similar urban and peri-urban environments.

CONCLUSION

This study presents a comprehensive geostatistical and multivariate evaluation of soil fertility within the Wukari urban landscape, integrating descriptive analysis, correlation structure, principal component analysis, sensitivity testing, spatial modeling, and classification mapping into a unified systems-based framework. The findings demonstrate that soil fertility gradients in the study area are fundamentally governed by exchange-complex dynamics, with calcium exerting dominant control over total exchangeable bases and effective cation exchange capacity. The PCA-derived Soil Fertility Index confirms that fertility differentiation is structured primarily by exchange-capacity magnitude rather than balanced NPK variability. Organic–nitrogen interactions function as secondary contributors, while phosphorus exhibits relative independence from the dominant fertility axis.

Spatial diagnostics reveal a chemically structured yet spatially patchy fertility system. Moderate spatial dependence of exchange variables, combined with weak global autocorrelation, indicates localized heterogeneity rather than broad regional clustering. The SFI classification further shows that moderate-to-high fertility conditions dominate more than half of the landscape (54.26%), while low-fertility zones remain substantial (34.54%) but spatially dispersed. These patterns underscore the importance of site-specific nutrient management within urban soil systems.

The sensitivity analysis provides a critical methodological contribution, demonstrating that the SFI is structurally anchored in exchange-complex variables and remains robust under removal of non-dominant indicators. This strengthens the defensibility of PCA-derived fertility indices and offers a replicable framework for multivariate fertility modeling in comparable environments. Collectively, the results move beyond conventional nutrient mapping by quantifying the hierarchical chemical architecture of soil fertility and its spatial manifestation. The study establishes that fertility variability in Wukari urban soils is chemically mediated, spatially heterogeneous, and exchange-capacity-driven—an insight with both scientific and practical implications for urban agricultural planning and targeted nutrient management.

Future research should integrate environmental covariates such as land-use patterns, elevation, slope, drainage conditions, and anthropogenic disturbance indices into spatial modeling frameworks. The application of redundancy analysis, canonical ordination techniques, or regression-kriging approaches would allow explicit quantification of environmental drivers controlling fertility gradients. Sensitivity-based modeling of weighted multi-criteria evaluation fertility indices could be developed as a complementary framework to the PCA-derived SFI. Comparative evaluation of statistically derived versus decision-weighted fertility indices would provide valuable insight into methodological robustness and spatial consistency. Temporal monitoring of fertility dynamics would enhance understanding of how urban land-use transitions influence exchange-complex evolution and nutrient balance over time. Finally, targeted investigation of localized cation imbalance zones—particularly areas exhibiting extreme Ca:Mg variability or elevated sodium indices could clarify potential structural or agronomic implications under intensified cultivation.

Funding

This work was funded by the Tertiary Education Trust Fund (TETfund) Nigeria, through Institution Based Research (IBR) intervention 2025. Federal University Wukari,

REFERENCES

A. A., S., M., A., & A. U., A. (2019). An Overview of Soil Fertility Degradation in Mubi Area, North-Eastern Part of Nigeria. *International Journal of Scientific and Research Publications (IJSRP)*, *9*(2), p8685. https://doi.org/10.29322/ijsrp.9.02.2019.p8685

Alshahrani, M. A., Ahmad, M., Laiq, M., & Nabi, M. (2025). Geostatistical analysis and multivariate assessment of groundwater quality. *Scientific Reports*, *15:7435*, 1–13.

An, X., Jin, W., Zhang, H., Liu, Y., & Zhang, M. (2022). Analysis of long-term wetland variations in China using land use / land cover dataset derived from Landsat images. *Ecological Indicators*, *145*(November), 109689. https://doi.org/10.1016/j.ecolind.2022.109689

Arunbose, S., Srinivas, Y., Rajkumar, S., Nair, N. C., & Kaliraj, S. (2021). Remote sensing, GIS and AHP techniques based investigation of groundwater potential zones in the Karumeniyar river basin, Tamil Nadu, southern India. *Groundwater for Sustainable Development*, *14*(January), 100586. https://doi.org/10.1016/j.gsd.2021.100586

Ayalew, G., Tiringo, T., Alemayehu, Y., Khebour, F., & Reichert, J. M. (2021). Spatial variability modeling of soil fertility for improved nutrient management in Northwest Ethiopia. *Arabian Journal of Geosciences*, *(2021) 14:*, 1–14. https://doi.org/https://doi.org/10.1007/s12517-021-08814-5 ORIGINAL

Ayodotun, B., Bamba, S., & Adio, A. (2019). *Vulnerability Assessment of West African Countries to Climate Change and Variability*. *January*. https://doi.org/10.4236/gep.2019.76002

Gavrilovic, M., Azar, J. C., Lindblad, J., Wahlby, C., Bengtsson, E., Busch, C., & Carlbom, I. B. (2013). Blind color decomposition of histological images. *IEEE Transactions on Medical Imaging*, *32*(6), 983–994. https://doi.org/10.1109/TMI.2013.2239655

I. D., G., B. A., H., M. S., B., & N., J. (2021). Analysis of Soil Physiochemical Properties on Different Land_use in Mubi North Local Government Area, Adamawa State, Nigeria. *International Journal of Research and Innovation in Social Science*, *05*(09), 687–696. https://doi.org/10.47772/ijriss.2021.5941

I. K, Y. (2023). Structural Analysis of Shrub – Tree Species in Yobe State, North Eastern Nigeria. *Arid-Zone Journal of Basic & Applied Research*, *2*(3), 1–14. https://doi.org/10.55639/607.070605

Jajere, A. A. (2023). *Analysis of Hadeja-Nguru Wetlands Vegetation and Surface water response to rainfall variability Analysis of Hadeja-Nguru Wetlands Vegetation and Surface water response to rainfall variability*. 1–19.

Jauhari, I., Aziz, A., Utami, R., & Ajizah, N. (2025). Management of Excellent Madrasa Program in Increasing Institutional Competitiveness. *Jurnal Ilmu Pendidikan Islam*, *21*(2), 93–108. https://doi.org/https://doi.org/10.54069/attaqwa.v21i2.976 Management

Keshavarzi, A., Caires, S. A. De, Sintim, H. Y., Kaya, F., Yaw, N., Yeboah, O. K., & Agyei, G. (2025). Spatial Variability and Management Zones : Leveraging Geostatistics and Fuzzy Clustering. *Journal of Soil Science and Plant Nutrition*, *25*(2), 3633–3651. https://doi.org/10.1007/s42729-025-02357-4

Kila, S. E. P. A. A., & Ragasan, L. I. A. R. U. L. P. (2026). SPATIAL VARIABILITY OF SOIL QUALITY UNDER DIVERSE LAND USE SYSTEMS IN TROPICAL COASTAL ENVIRONMENTS : A CASE STUDY FROM INDIA. *Journal of Landscape Ecology*, *Vol: 19 /*(3). https://doi.org/10.2478/jlecol-2026-0024

Marchetti, A., Piccini, C., Francaviglia, R., & Mabit, L. (2012). Spatial Distribution of Soil Organic Matter Using Geostatistics : A Key Indicator to Assess Soil Degradation Status in Central Italy ∗ 1. *Pedosphere 22(2): 230–242, 2012*, *22*(Dm), 230–242.

Mosavi, A., Sajedi-Hosseini, F., Choubin, B., Taromideh, F., Rahi, G., & Dineva, A. A. (2020). Susceptibility mapping of soil water erosion using machine learning models. *Water (Switzerland)*, *12*(7), 1–17. https://doi.org/10.3390/w12071995

Özen, F. (2019). Evaluation of soil fertility in citrus planted areas by geostatistics analysis method. *Eurasian Soil Science*, *8*(4), 351–363. https://doi.org/10.18393/ejss.616689

Özyazici, M. A., Dengiz, O., Sa, M., & Erkoçak, A. (2017). Mapping and assessment-based modeling of soil fertility differences in the central and eastern parts of the Black Sea region using GIS and geostatistical approaches. *Arab J Geosci (2017) 10:45*. https://doi.org/10.1007/s12517-016-2819-6

Parvizi, Y., & Fatehi, S. (2025). Geospatial digital mapping of soil organic carbon using machine learning and geostatistical methods in different land uses. *Scientific African*, 1–16.

Ramzan, S., Wani, M. A., & Bhat, M. A. (2017). Assessment of Spatial Variability of Soil Fertility Parameters Using Geospatial Techniques in Temperate Himalayas. *International Journal of Geosciences, 2017, 8, 1251-1263*, *2017*, 1251–1263. https://doi.org/10.4236/ijg.2017.810072

Sharma, R., Mishra, D. R., & Levi, M. R. (2022). *Remote Sensing of Surface and Subsurface Soil Organic Carbon in Tidal Remote Sensing of Surface and Subsurface Soil Organic Carbon in Tidal Wetlands : A Review and Ideas for Future Research*. *June*. https://doi.org/10.3390/rs14122940

Sharma, R. P., Chattaraj, S., Vasu, D., Karthikeyan, K., Tiwary, P., Naitam, R. K., Dash, B., Tiwari, G., Jangir, A., Daripa, A., Singh, S. K., & Anantwar, S. G. (2020). Spatial variability assessment of soil fertility in black soils of central India using geostatistical modeling Spatial variability assessment of soil fertility in black soils of. *Archives of Agronomy and Soil Science ISSN:* https://doi.org/10.1080/03650340.2020.1766678

Shokr, M. S., Jalhoum, M. E. M., & Sayed, A. S. A. (2025). Assessment of soil quality in arid zones using principal component analysis and GIS-based modeling. *PLOS One*, *66*, 1–25. https://doi.org/10.1371/journal.pone.0337063

Singh, A. (2026). Egyptian Journal of Soil Science. *Egyptian Journal of Soil Science*, *66*(1), 1–24. https://doi.org/10.21608/ejss.2026.445040.2455

Sun, C., Feng, X., Fu, B., & Ma, S. (2023). Desertification vulnerability under accelerated dryland expansion. *Land Degradation and Development*, *34*(7), 1991–2004. https://doi.org/10.1002/ldr.4584

Venkateswarlu, M., Rallapalli, S., Singh, A., & Chalapathi, G. S. S. (2025). Macro and micronutrient based soil fertility zonation using fuzzy logic and geospatial techniques. *Scientific African*, *15:26772* |, 1–22.

Wang, S., Zhou, M., & Zhuang, Q. (2021). *Prediction Potential of Remote Sensing-Related Variables in the Topsoil Organic Carbon Density of Liaohekou Coastal Wetlands , Northeast China*. 1–15.

Yakub, W., Muhammad, A., Ibrahim, R., & Bawa, D. B. (2022). Spatial Variability of Soil Organic Carbon, Total Nitrogen and Soil pH In Soils of Wukari Local Government Area Taraba State, Nigeria. *Asian Journal of Agriculture*, *5*(1), 1–11.

Zeraatpisheh, M., Ayoubi, S., & Sulieman, M. (2025). Determining the spatial distribution of soil properties using the environmental covariates and multivariate statistical analysis : a case study in semi-arid regions of. *JOURNAL OF ARID LAND*. https://doi.org/https://doi.org/10.1007/s40333-019-0059-9